Observation of the Planar Nernst Effect in Permalloy and Nickel Thin Films with In-Plane Thermal Gradients

A. D. Avery,[1] M. R. Pufall,[2] and B. L. Zink[1]

[1]*Department of Physics and Astronomy, University of Denver, Denver, Colorado 80208, USA*
[2]*Electromagnetics Division, National Institute of Standards and Technology, Boulder, Colorado 80305, USA*

(Received 26 June 2012; published 7 November 2012)

We present experimental evidence of a transverse thermopower, or planar Nernst effect, in ferromagnetic metal thin films driven by thermal gradients applied in the plane of the films. Samples of 20 nm thick Ni and $Ni_{80}Fe_{20}$ were deposited on 500 nm thick suspended Si-N thermal isolation platforms with integrated platinum strips designed originally to allow measurement of thermally generated spin currents (the spin Seebeck effect). The low thermal conductivity of the thin supporting Si-N structure results in an essentially 2D geometry that approaches the *zero substrate* limit, dramatically reducing the contribution of thermal gradients perpendicular to the sample plane typically found in similar experiments on bulk substrates. The voltage on the platinum strips generated transverse to the applied thermal gradient (V_T) is linear with increasing $\triangle T$ and exhibits a sign reversal on hot and cold sides of the sample. However, V_T is always even in applied magnetic field and shows a $\sin\theta\cos\theta$ angular dependence, both key indicators of the planar Nernst effect. Within the 5 nV estimated error of our experiment there is no evidence of a signal from the spin Seebeck effect, which would have $\cos\theta$ angular dependence, suggesting a reduced spin Seebeck coefficient in a planar, entirely thin-film geometry.

DOI: 10.1103/PhysRevLett.109.196602 PACS numbers: 72.15.Jf, 85.75.−d, 85.80.−b, 85.85.+j

The reliable generation of pure spin currents, transport of angular momentum without movement of charge, is an important step toward a future spin-based nanoelectronics model that could allow computer speed and power consumption to move past limitations of current technologies [1–4]. One possible route toward a source for pure spin currents has been termed the spin Seebeck effect (SSE) [5,6], where application of a thermal gradient to a ferromagnet causes a spin imbalance which can drive pure spin currents into normal metal contacts. Such coupling between spin and thermal excitations is a rapidly growing area of research that has been given the name *spin caloritronics*, [7,8] and has stimulated interest in a range of thermoelectric and magnetothermoelectric effects.

Some form of the SSE has now been reported for metallic, semiconducting, and insulating ferromagnetic (FM) films grown on thick substrates [5,9–11]. However, the physical mechanisms responsible for the observed effects are still being debated among both experimentalists and theorists. A key piece of the puzzle could be found in the so-called *longitudinal* spin Seebeck effect [11,12]. In the SSE as originally discussed, shown schematically in Fig. 1(a), a thermal gradient (∇T) applied along a sample in the $\hat{x}$ direction creates a spin current that flows perpendicularly into normal metal contacts at the sample ends in the $\hat{z}$ direction. For metals with large spin-orbit coupling such as Pt [13], the inverse spin Hall effect (ISHE) [14,15] causes a charge voltage to appear across the metal contact in the $\hat{y}$ direction. In contrast, observations of the longitudinal SSE were made with applied heat perpendicular to the sample, substrate, and detector strip, so that the resulting ∇T is also in the $\hat{z}$ direction [11,12]. This modified geometry can generate signals as large or larger than those reported in the original SSE observations. Other reports suggest that the SSE signal is strongly dependent on the thermal conductivity of or phonon flow in the bulk substrate itself [16,17]. Furthermore, recent work on

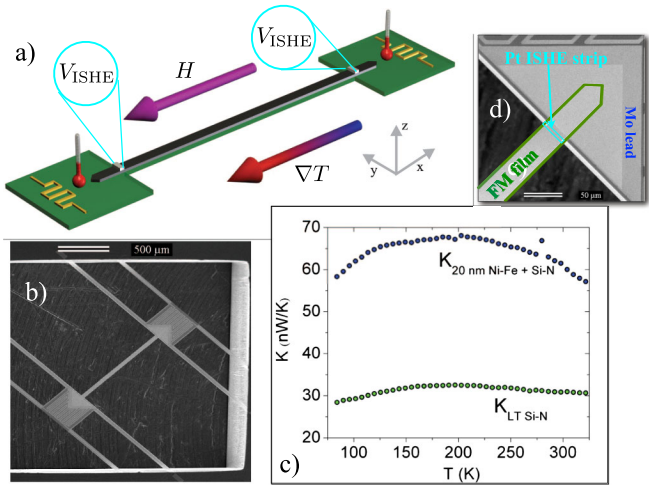

FIG. 1 (color online). (a) Schematic of the thermal isolation platform with ∇T and H applied in the negative x direction, (b) SEM micrograph of the platform, and (c) plot of thermal conductance vs T for a Si-N bridge and a 20 nm Ni-Fe film deposited on a Si-N bridge. (d) SEM micrograph of one island shows a triangle-shaped lead for measuring film resistance and thermopower, false color outlines show a 20 nm thick Ni-Fe film and a 10 nm thick Pt spin detector.

spin-dependent transport in thin film nanostructures on bulk substrates has underscored the difficulty in understanding thermal gradients applied to thin films on thick substrates [18]. The size of the longitudinal SSE coefficients, along with the uncertainty that arises concerning the direction of the actual thermal gradient generated on a thin film placed on a thick substrate with overall thermal conductance that is at least a factor of 1000× larger than the contribution of the magnetic sample [18], suggests that the early SSE experiments may have also been affected by both the longitudinal SSE and an anomalous Nernst effect contribution.

Progress toward a complete physical picture requires experiments that can clearly distinguish signals caused by known thermoelectric or magnetothermoelectric effects. For example, in addition to the anomalous Nernst effect that can mimic the signatures of the SSE when out-of-plane thermal gradients develop, a transverse thermopower, or planar Nernst effect (PNE), is known in ferromagnetic semiconductors and metals [19,20]. This effect, caused by the same spin-dependent scattering that generates both anisotropic magnetoresistance (AMR) and the standard thermopower, can add a transverse voltage generated by the ferromagnetic material itself in response to ∇T to the voltage potentially generated by the SSE. However, these effects can be separated by their angular dependence. The ISHE used to detect the SSE should produce no voltage when the magnetization is parallel to the Pt strip, and an opposite sign when the applied field reverses the magnetization, leading to a $\cos\theta$ dependence, where θ is the angle between the applied magnetic field (assumed parallel to magnetization M in these samples) and the ∇T vectors. The PNE instead shows a $\sin\theta\cos\theta$ dependence.

In this Letter we present the first results from a novel approach for examining the spin Seebeck and related effects in ferromagnetic metal films. By using micromachined suspended Si-N membranes, we are able to perform thermoelectric experiments that approach the zero substrate limit [21–23]. The 500 nm thick thermal isolation platforms reduce thermal conduction through the substrate by at least 1000× compared to experiments performed using bulk substrates. This confinement to the plane of the platform and film ensures a ∇T in the x or y direction only. The experiment therefore explores the SSE in a truly planar geometry. The resulting V_T shows some features previously thought to be unique to SSE, but has a field dependence in complete agreement with the PNE, observed here in ferromagnetic metal thin films.

Figure 1 shows a schematic and SEM micrographs of the thermal isolation platform. This platform consists of two suspended Si-N islands connected by a $35 \times 800\ \mu\text{m}^2$ bridge [Fig. 1(b)]. A heater and thermometer is lithographically patterned on each island. An additional thermometer is patterned on the frame for monitoring T of the heat bath. The film is deposited on the bridge and overlaps triangle-shaped Mo leads on each island for making measurements of film resistance and thermopower [see Fig. 1(d)].

The thermal platforms are based on structures we use to measure thermal conductivity and the conventional Seebeck effect in thin films and nanostructures [21–23]. The key addition required to probe thermal spin currents are Pt strips to provide detection of spin via the ISHE [14,15]. The sample layer, Pt spin detectors, and their Au leads (with a thin titanium sticking layer) are deposited in three separate steps through lithographically patterned photoresist lift-off masks. This lift-off layer is removed after each deposition and the exposed surfaces are rf sputter-cleaned for several minutes to ensure reliable contact between layers. We use deep trench silicon etching to remove the bulk substrate and thermally isolate the platform. After fabrication, the platform is mounted in a fully radiation shielded Au-plated box in a sample-in-vacuum liquid nitrogen cryostat. ∇T is created along the bridge by applying a known current to the heater on one island. T of each island and the reference T of the frame are determined from the resistance of each thermometer. Every thermometer used is individually calibrated from measurements of R vs T over the desired range.

To test for the presence of SSE or PNE, we monitor the transverse voltage (V_T) across the Pt strips in response to applied ∇T. When measuring V_T we typically observe background voltages of up to several μV that drift slightly over a several minute time-scale, even without an applied ∇T. This expected background is due to thermovoltages produced by conventional Seebeck effects in experimental wiring [24], and its effect can be safely removed from our data. Figure 2 shows an example data point taken at 100 Oe (with $\theta = 0$) for one Pt detector. All measurements were conducted at a base T of 276 K. V_T is measured while the sample heater is cycled on and off. The low thermal mass of the platform allows the sample to reach thermal equilibrium in <1 s. After subtracting a linear fit to the unheated data to correct for thermal drift, we average 20 trials to increase the signal-to-noise ratio. We repeat the measurement after reversing ∇T by heating the opposite island. This allows comparison of the responses for the same Pt strip when hot or cold.

The thermal isolation platforms are designed to be as symmetric as possible to eliminate thermovoltages from unmatched thermal gradients in either direction along the legs, ∇T_y. However, variation in the platform materials can cause asymmetries and background thermovoltages that contribute to the measured V_T signal. Measurement of V_T while equally heating both islands so that $\nabla T_x = 0$ allows us to determine this background. Once identified [Fig. 2(c)], we subtract it from the voltages measured while heating each island separately ($V_{\text{hot+background}} - V_{\text{background}} = V_{\text{hot}}$). The response of an example detector to a ∇T_x, is shown in Fig. 2(d), when at the hot and cold end

of a sample Ni-Fe film. Note that these signals are symmetric about zero and of opposite sign, demonstrating the spatial reversal thought to be a key signature of the SSE.

Figure 3 shows V_T as a function of increasing ΔT measured at 100 Oe (at $\theta = 0$) for both detectors on a single film when hot and cold, as well as points at $\Delta T = 50$ K for the respective detectors of four additional Ni-Fe films. Though there is a spread in values among the various Pt strips measured, V_T for all samples is linear with ΔT_x as expected. The voltages are symmetric about zero for each detector and as shown in Fig. 2, the sign of the voltage measured at opposite ends of the film is reversed. These patterns are present in all 12 detectors on 6 Ni-Fe films and 3 detectors on 2 Ni films we measured. All these samples exhibited magnetic field dependence. Figure 3(b) shows an example V_T versus applied magnetic field (H) for a Ni-Fe film. We also tested a platform with a 20 nm thick Au film (see Supplemental Material [25]) which served as a nonmagnetic control and showed neither spatial dependence nor magnetic field dependence.

Figure 4(a) displays AMR vs H for a Ni film (Ni-a) and Fig. 4(b) shows V_T versus H for a detector when hot and cold in another Ni film (Ni-b). Like AMR, the field dependence of V_T for both Ni-Fe [shown in Fig. 3(b)] and Ni is even. This differs from previous measurements of films on bulk substrates where the field dependence reported for the SSE resembled an M-H curve [5,9,11]. The coercivity in Ni-Fe and Ni are similar to the AMR peaks measured on these and additional films (Ni-Fe not shown). The background corrected V_T signal for each detector is again approximately symmetric about $V_T = 0$ in both saturation value and peak magnitude [26].

Figures 4(c)–4(e) presents angular dependence of V_T for a Ni film. Figures 4(c) and 4(d) show V_T for one detector on the Ni-b film when cold and hot at values of θ spaced by 45 degree increments (data shown for only one direction of H sweep for clarity). When the detector is cold, V_T is positive for $\theta = 45°$ and 225° with a larger saturation value when compared to saturated values at $\theta = 0°$ and 180°. Rotating the sample an additional 90° generated negative saturation values for $\theta = 135°$ and 315°. Near $M = 0$, V_T values are similar for all angles. Reversal of the applied ∇T changes the detector from cold to hot, but as shown in insets to Fig. 4(e), also inverts the sign of the PNE component. This effect is shown in Fig. 4(d), where the pattern of saturated values is reversed from Fig. 4(c). Figure 4(e) clarifies this pattern and the overall angular dependence by plotting the V_T in a saturating field of 200 Oe vs θ for the detector when both cold and hot. Both match the $\sin\theta\cos\theta$ dependence of the PNE extremely well, though with a *field-independent* positive (negative) constant component added when the detector is cold (hot). Again, note the hot data appear to be proportional to $-\sin\theta\cos\theta$ simply due to the negative sign introduced by the reversed ∇T. This sign change is only relevant for the PNE component of V_T, since the pattern of positive V_T for the cold detector and negative V_T for the hot detector is present when ∇T is not reversed.

Data in Fig. 4 clearly indicate that the field dependence of the signals in our experiment is entirely explained by the planar Nernst effect. The component of V_T responsible for the sign change on the hot and cold ends of the sample has

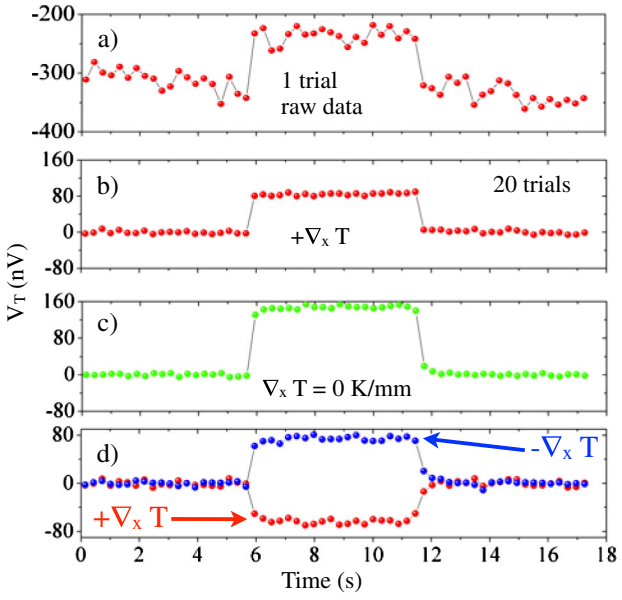

FIG. 2 (color online). (a) Example raw data for V_T across a Pt detector. (b) Averaged data when hot ($\nabla_x T = 62.5$ K/mm, and (c) when both sides of the film heated equally leaving only the background thermovoltage generated by ∇T_y. (d) Hot and cold measurements ($\nabla_x = \pm 62.5$ K/mm) after subtracting the ∇T_y contribution. For all measurements, the heater is cycled on at 6 seconds and off at 11 seconds.

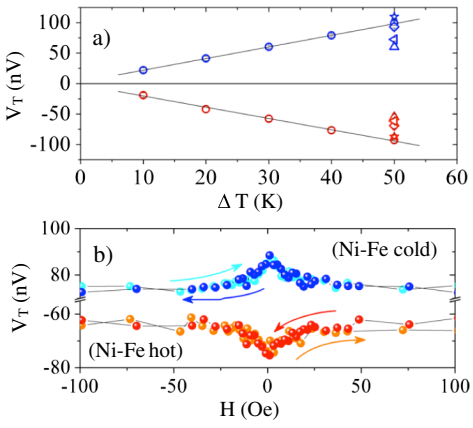

FIG. 3 (color online). V_T versus ΔT for Ni-Fe ($H = 100$ Oe, $\theta = 0$). (a) V_T for one detector when hot and cold with a linear fit. Additional points at $\Delta T = 50$ K are for the same detector on four additional Ni-Fe films. The same trends occur for the other Pt detector (not shown). (b) V_T versus H (applied in the $\pm\hat{x}$ direction) for one detector on a Ni-Fe film when hot and cold for up and down H sweeps.

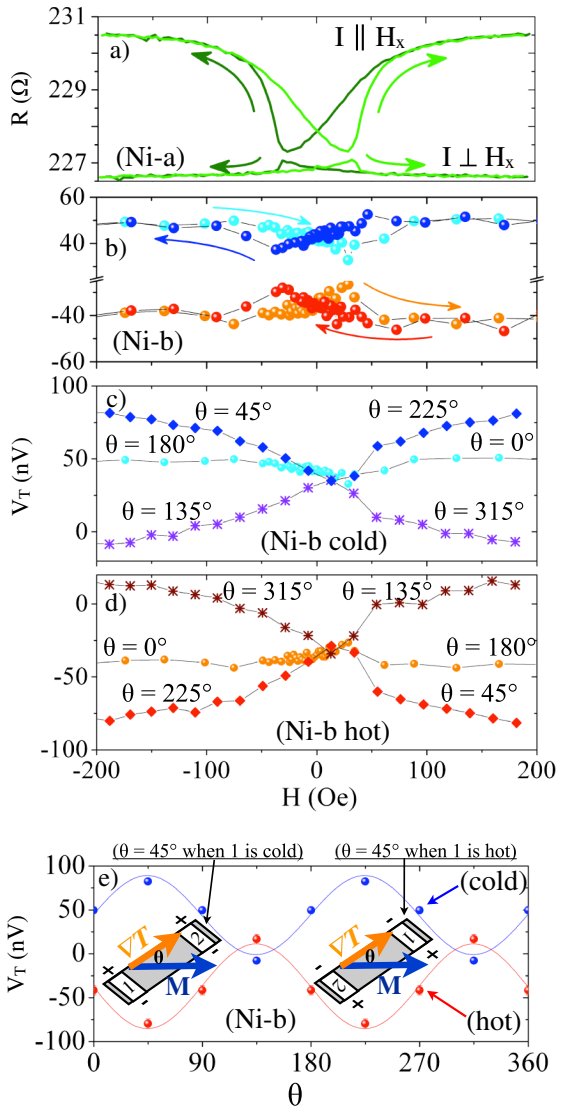

FIG. 4 (color online). (a) AMR data for a Ni-a. (b) V_T versus H for one detector on Ni-b when hot and cold for up and down H sweeps. (c) V_T versus H for Ni-b when cold for one sweep direction at various θ (the angle between M and ∇T) and (d) when hot. (e) V_T vs θ for Ni-b when the detector is hot and cold with $\sin\theta\cos\theta$ fit. Data when hot appear reversed due to the sign change introduced by reversing ∇T *Insets:* Schematics show the sign change for V_T when ∇T is reversed.

no field dependence, and is therefore very difficult to interpret as due to a spin current flowing from the ferromagnet into the Pt ISHE spin detectors. Therefore, within the error of our experiment, there is no evidence of thermally generated spin currents, which would add a component to V_T with a $\cos\theta$ angular dependence. This puts an upper limit on the size of the SSE in our planar geometry.

Before discussing the size of the SSE coefficient (S_s), we consider other reasons why the SSE might not appear in our experiment. The first concern is the interface between the FM and Pt ISHE detector. Though we have taken steps to assure a high quality contact (rf cleaning of the FM surface before deposition of Pt at pressures of $\approx 10^{-7}$ Torr), it is possible that the interface unintentionally limits the flow of spins into the Pt. It is difficult to probe the quality of the interface directly in our structures, though electrical resistance measurements in various configurations rule out a large contact resistance that would suggest poor transparency between the Pt and FM. The second concern is that the Mo contacts at the ends of the sample (several μm distant from the Pt) increase the electrical conductance of the structure and partially reduce any transverse voltage. We have estimated the size of this reduction based on the relation between measured longitudinal thermopower (described elsewhere [27]) and the PNE to be $\sim$0.4.

Previous reports for Ni-Fe and Ni were $S_{s,\mathrm{Ni-Fe}} = -6 \times 10^{-11}$ V/K and $S_{s,\mathrm{Ni}} = 5 \times 10^{-11}$ V/K [28], where $S_s = -(2/\theta_{\mathrm{Pt}}\eta_{\mathrm{FM-Pt}})(d_{\mathrm{Pt}}/L_{\mathrm{Pt}})(V_{\mathrm{ISHE}}/\Delta T)$. Here θ_{Pt} is the spin-Hall angle, $\eta_{\mathrm{FM-Pt}}$ is the spin injection efficiency, d_{Pt} and L_{Pt} are thickness and length of the Pt strip, and V_{ISHE} is the size of the voltage generated on the hot end of the saturated FM sample. Using the geometry of our micromachined platform, $\Delta T = 50$ K, and assuming the same values of $\theta_{\mathrm{Pt}} = 0.08$ and $\eta_{\mathrm{FM-Pt}} = 0.16$ and S_s as the previous reports, we would expect an SSE contribution of 56 nV in Ni and 67 nV in Ni-Fe [note that this should appear as an antisymmetric component in Figs. 3(b) and 4(b) of $2V_{\mathrm{ISHE}}$, due to the expected $\cos\theta$ dependence]. If the Mo features partially short this voltage by the expected factor of 0.4, we would still expect a voltage from the SSE of $2V_{\mathrm{ISHE}} \sim 50$ nV. In fact, any SSE component in our experiment is less than the experimental error of ≈ 5 nV. If present, the spin Seebeck effect is significantly reduced in our planar geometry.

In summary, we have used a novel technique to probe the SSE and PNE in the zero substrate limit. Though the linear dependence of V_T on $\triangle T$ and the spatial dependence are similar to SSE measurements on films supported by bulk substrates, the magnetic field dependence is entirely explained by the PNE. The upper limit on the SSE coefficient in our experiment is at least an order of magnitude smaller than previous measurements on FM metals on bulk substrates.

We gratefully acknowledge support from the Nanoelectronics Research Corporation through the Western Institute of Nanoelectronics and the NSF CAREER Grant No. (DMR-0847796). We also thank J. Beall, G. Hilton, D. Schmidt, and A. Fox for fabrication advice and assistance, and S. Mason, D. Bassett, D. Wei, and J. Rauch for assistance in the lab.

[1] S. D. Bader and S. S. P. Parkin, Annu. Rev. Condens. Matter Phys. **1**, 71 (2010).
[2] D. D. Awschalom and M. E. Flatté, Nat. Phys. **3**, 153 (2007).

[3] S. A. Wolf, D. D. Awschalom, R. A. Buhrman, J. M. Daughton, S. Von Molnar, M. L. Roukes, A. Y. Chtchelkanova, and D. M. Treger, Science **294**, 1488 (2001).
[4] I. Žutić, J. Fabian, and S. D. Sarma, Rev. Mod. Phys. **76**, 323 (2004).
[5] K. Uchida, S. Takahashi, K. Harii, J. Ieda, W. Koshibae, K. Ando, S. Maekawa, and E. Saitoh, Nature (London) **455**, 778 (2008).
[6] J. Sinova, Nature Mater. **9**, 880 (2010).
[7] G. E. W. Bauer, E. Saitoh, and B. J. van Wees, Nature Mater. **11**, 391 (2012).
[8] G. E. W. Bauer, A. H. MacDonald, and S. Maekawa, Solid State Commun. **150**, 459 (2010).
[9] C. M. Jaworski, J. Yang, S. Mack, D. D. Awschalom, J. P. Heremans, and R. C. Myers, Nature Mater. **9**, 898 (2010).
[10] K. Uchida, J. Xiao, H. Adachi, J. Ohe, S. Takahashi, J. Ieda, T. Ota, Y. Kajiwara, H. Umezawa, H. Kawai, G. E. W. Bauer, S. Maekawa, and E. Saitoh, Nature Mater. **9**, 894 (2010).
[11] K. Uchida, H. Adachi, T. Ota, H. Nakayama, S. Maekawa, and E. Saitoh, Appl. Phys. Lett. **97**, 172505 (2010).
[12] K. Uchida, T. Nonaka, T. Ota, and E. Saitoh, Appl. Phys. Lett. **97**, 262504 (2010).
[13] O. Mosendz, J. E. Pearson, F. Y. Fradin, G. E. W. Bauer, S. D. Bader, and A. Hoffmann, Phys. Rev. Lett. **104**, 046601 (2010).
[14] J. E. Hirsch, Phys. Rev. Lett. **83**, 1834 (1999).
[15] E. Saitoh, M. Ueda, H. Miyajima, and G. Tatara, Appl. Phys. Lett. **88**, 182509 (2006).
[16] C. M. Jaworski, J. Yang, S. Mack, D. D. Awschalom, R. C. Myers, and J. P. Heremans, Phys. Rev. Lett. **106**, 186601 (2011).
[17] H. Adachi, K. ichi Uchida, E. Saitoh, J. ichiro Ohe, S. Takahashi, and S. Maekawa, Appl. Phys. Lett. **97**, 252506 (2010).
[18] S. Y. Huang, W. G. Wang, S. F. Lee, J. Kwo, and C. L. Chien, Phys. Rev. Lett. **107**, 216604 (2011).
[19] Y. Pu, E. Johnston-Halperin, D. D. Awschalom, and J. Shi, Phys. Rev. Lett. **97**, 036601 (2006).
[20] V. D. Ky, Phys. Status Solidi (b) **22**, 729 (1967).
[21] R. Sultan, A. D. Avery, G. Stiehl, and B. L. Zink, J. Appl. Phys. **105**, 043501 (2009).
[22] B. L. Zink, A. D. Avery, R. Sultan, D. Bassett, and M. R. Pufall, Solid State Commun. **150**, 514 (2010).
[23] A. D. Avery, R. Sultan, D. Bassett, D. Wei, and B. L. Zink, Phys. Rev. B **83**, 100401 (2011).
[24] This background thermovoltage occurs mainly due to the temperature gradient between the sample held at 276 K and the room-temperature end of the wiring which can fluctuate several degrees. Any length difference in the ~0.5 m long manganin twisted pairs will produce imperfect cancellation of the thermovoltage developed across these wires and cause the thermoelectric background.
[25] See Supplemental Material at http://link.aps.org/supplemental/10.1103/PhysRevLett.109.196602 for data on the nonmagnetic control sample.
[26] The background with ∇T_y only was also field dependent. This is caused by the magnetothermopower of the film when heated in the y direction. A paper by A. D. Avery, M. R. Pufall, and B. L. Zink presenting magnetothermopower and AMR in FM films will appear.
[27] A. D. Avery, M. R. Pufall, and B. L. Zink (to be published).
[28] K. Uchida, T. Ota, K. Harii, K. Ando, H. Nakayama, and E. Saitoh, J. Appl. Phys. **107**, 09A951 (2010).